Transfer Phenomena in Non-Darcy Bidisperse Porous Media

TEODOR GROSAN
Department of Mathematics
Babes Bolyai University
M. Kogalniceanu Str., No. 1, 400084, Cluj-Napoca
ROMANIA
tgrosan@math.ubbcluj.ro

IOAN POP
Department of Mathematics
Babes Bolyai University
M. Kogalniceanu Str., No. 1, 400084, Cluj-Napoca
ROMANIA
popm.ioan@yahoo.co.uk

FLAVIUS O. PATRULESCU
Tiberiu Popoviciu Institute of Numerical Analysis, Romanian Academy
Str. Fântânele nr. 57, ap. 67-68, 400320 Cluj-Napoca
ROMANIA
fpatrulescu@ictp.acad.ro

Abstract: - This paper presents the mathematical model for the free convection in a non-Darcy bidisperse porous medium. An appropriate mathematical model taken into account the Brinkman and Darcy-Forchheimer terms is proposed. A boundary layer problem and two cavity problems are discussed. Systems of partial differential equations containing inertial, inter-phase momentum, thermal diffusivity ratio, thermal conductivity ratio, permeability ratio, modified thermal capacity and convection parameters are solved numerically. The characteristics of the flow and heat transfer are discussed and presented graphically.

Key-Words: - Bidisperse porous media, Non-Darcy porous media, Convective heat transfer.

1 Introduction

In the last years, there has been much interest in multiple porosity materials [1], [2]. A standard porous medium is formed by the solid matrix and voids filled with fluid. However, there are cases when a solid body may have a double porosity structure (bidisperse porous medium -BDPM). In these cases the solid structure of the medium is composed of clusters of large particles that are agglomerations of small particles (see Fig.1). Thus, a BDPM is a standard porous medium in which the solid phase is replaced by another porous medium.

An example of bidisperse porous medium is given in Fig. 2, where beds of porous or fractured rocks are depicted. There is a macro-porosity, ϕ_1,(voids between rocks) but also a micro-porosity, ϕ_2, which is linked with fissures and pores in the solid skeleton. In this kind of geological systems the macro-porosity suffers modifications due to the action of precipitations and freezing–thawing cycles.

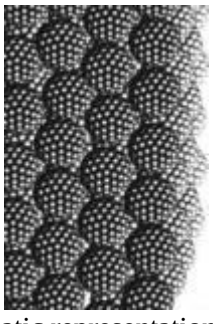

Fig. 1. Schematic representation of bidisperse porous media (Rees et al., 2008)

Several applications of BDMP are related to thermal insulation, [2], and heat pipes technologies [3], see Fig. 3. This is due to the fact that the Rayleigh number is much higher for a BDPM that for a classical porous medium and that the maximum heat

load of bidisperse wick is higher than that for the monoporous wick.

Fig. 2. A landfill containing piles of fractured and porous rocks (Szczygieł, 2006)

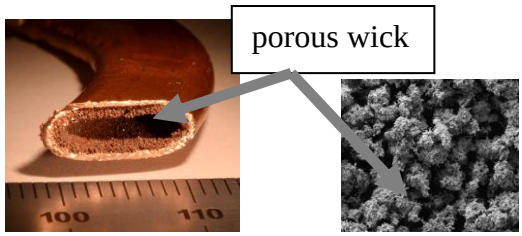

Fig. 3. Cross section of a heat pipe for cooling the CPU of a laptop computer (Wikipedia) and the bidisperse porous wick [4].

Other applications of the bidisperse porous media are related to catalytic chemistry, see Fig. 4 [4] and methane recovery from coal deposits, see Fig. 5, [5].

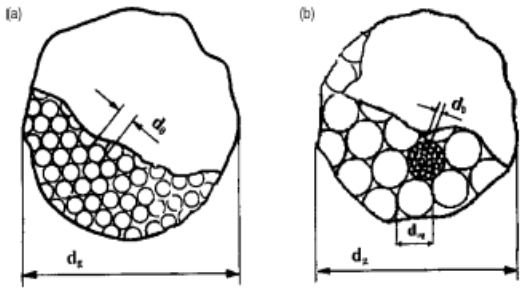

Fig. 4. a) mondisperse catalyst b) bidisperse catalyst.

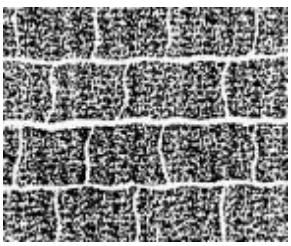

Fig. 5. Bidisperse coal bad

In the present paper the mathematical models for non-Darcy porous media (macro and micro phases) are studied.

2 Problem Formulation

One of the most complexes mathematical model for a bidisperse porous medium is given by [2] where the inertial Darcy-Forchheimer terms are added:

Continuity equation for the macro scale:

$$\frac{\partial u_f}{\partial x}+\frac{\partial v_f}{\partial y}=0=0 \tag{1.1}$$

Continuity equation for the micro scale:

$$\frac{\partial u_p}{\partial x}+\frac{\partial v_p}{\partial y}=0 \tag{1.2}$$

Momentum equations for the macro scale:

$$\begin{aligned}\frac{\partial p}{\partial x}=&-\frac{\mu}{K_f}u_f\left(1+\frac{\rho K_f'}{\mu}\left|\mathbf{v}_f\right|\right)-\zeta\left(u_f-u_p\right)\\&+\tilde{\mu}\left(\frac{\partial^2 u_f}{\partial x^2}+\frac{\partial^2 u_f}{\partial y^2}\right)\end{aligned} \tag{1.3}$$

$$\begin{aligned}\frac{\partial p}{\partial y}=&-\frac{\mu}{K_f}v_f\left(1+\frac{\rho K_f'}{\mu}\left|\mathbf{v}_f\right|\right)+\zeta\left(v_f-v_p\right)\\&+\tilde{\mu}\left(\frac{\partial^2 v_f}{\partial x^2}+\frac{\partial^2 v_f}{\partial y^2}\right)\\&+\rho g\,\hat{\beta}(T_F-T_0)\end{aligned} \tag{1.4}$$

Momentum equations for the micro scale:

$$\begin{aligned}\frac{\partial p}{\partial x}=&-\frac{\mu}{K_f}u_p\left(1+\frac{\rho K_f'}{\mu}\left|\mathbf{v}_p\right|\right)-\zeta\left(u_p-u_p\right)\\&+\tilde{\mu}\left(\frac{\partial^2 u_p}{\partial x^2}+\frac{\partial^2 u_p}{\partial y^2}\right)\end{aligned} \tag{1.5}$$

$$\begin{aligned}\frac{\partial p}{\partial y}=&-\frac{\mu}{K_f}v_p\left(1+\frac{\rho K_f'}{\mu}\left|\mathbf{v}_p\right|\right)+\zeta\left(v_p-v_f\right)\\&+\tilde{\mu}\left(\frac{\partial^2 v_p}{\partial x^2}+\frac{\partial^2 v_p}{\partial y^2}\right)\\&+\rho g\,\hat{\beta}(T_F-T_0)\end{aligned} \tag{1.6}$$

where $|\mathbf{v}_\mathrm{f}|=(u_f^2+v_f^2)^{1/2}$ and $\left|\mathbf{v}_p\right|=(u_p^2+v_p^2)^{1/2}$ and

$$T_F=\frac{\phi\,T_f+(1-\phi)\mathcal{E}T_p}{\phi+(1-\phi)\mathcal{E}} \tag{1.7}$$

Momentum equation for the macro scale:

$$\begin{aligned}&\phi(\rho c)_f\left(u_f\frac{\partial T_f}{\partial x}+v_f\frac{\partial T_f}{\partial y}\right)\\&\qquad=\phi k_f\Delta\,T_f+h\left(T_p-T_f\right)\end{aligned} \tag{1.8}$$

Momentum equation for the micro scale:

$$(1-\phi)(\rho c)_p\left(u_p\frac{\partial T_p}{\partial x}+v_p\frac{\partial T_p}{\partial y}\right) = (1-\phi)k_p\Delta T_p + +h\left(T_f-T_p\right) \quad (1.9)$$

where *u* and *v* are the filtration velocity components along the *x* and *y* axes, respectively, v is the filtration velocity vector, *T* is the temperature, *p* is the pressure, *K* is the permeability, *K'* defines the inertial coefficient, *g* is the magnitude of the acceleration due to gravity, *k* is the thermal conductivity, *c* is the specific heat at constant pressure, *h* is interphase heat transfer coefficient, ϕ is the volume fraction of the *f*-phase, μ is the dynamic viscosity, ρ_F is the fluid density, ζ is the coefficient for momentum transfer between the two phases, μ̃ the effective viscosity of porous medium (as in – here the subscripts are dropped following the assumption that this parameter has equal values in all phases), $\mathcal{E}$ is the porosity within the *p*-phase and $\widehat{\beta}$ is the volumetric thermal expansion coefficient of the fluid with T_0 a reference temperature. The subscript *f* denotes the fracture phase (macropores) and *p* denotes the porous phase (micropores), respectively.

2.1 Natural convection from a vertical plate embedded in a non-Darcy bidisperse porous medium

We consider the steady free convection flow and heat transfer from a vertical plate embedded in a non-Darcy BDPM including only the Darcy_Forchheimer inertial term (see Fig. 1). It is assumed that the temperature of the plate, T_w, is constant, while far from the surface the ambient temperature of the saturated BDPM is T_∞ ($T_w > T_\infty$)

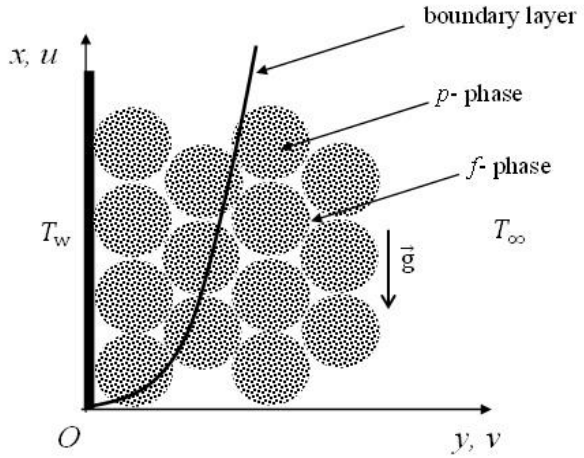

Fig. 1. Physical model and coordinate system

By using the boundary layer approximation (see Patrulescu et al. 2019)) the governing equations are:

$$\left(1+\sigma_f\right)\frac{\partial^2 f}{\partial\eta^2}-\sigma_f\beta\frac{\partial^2 g}{\partial\eta^2} +G_f^*\frac{\partial}{\partial\eta}\left(\left(\frac{\partial f}{\partial\eta}\right)^2\right)=\tau\frac{\partial\theta_f}{\partial\eta}+(1-\tau)\frac{\partial\theta_p}{\partial\eta} \quad (1.10)$$

$$-\sigma_f\frac{\partial^2 f}{\partial\eta^2}+\beta\left(\frac{1}{K_r}+\sigma_f\right)\frac{\partial^2 g}{\partial\eta^2} +\frac{\beta(1-\phi)G_p^*}{\phi K_r}\frac{\partial}{\partial\eta}\left(\left(\frac{\partial g}{\partial\eta}\right)^2\right) =\tau\frac{\partial\theta_f}{\partial\eta}+(1-\tau)\frac{\partial\theta_p}{\partial\eta} \quad (1.11)$$

$$\frac{\partial^2\theta_f}{\partial\eta^2}+\frac{\phi}{2}f\frac{\partial\theta_f}{\partial\eta} =\phi x\left(\frac{\partial f}{\partial\eta}\frac{\partial\theta_f}{\partial x}-\frac{\partial f}{\partial x}\frac{\partial\theta_f}{\partial\eta}\right)-Hx\left(\theta_p-\theta_f\right) \quad (1.12)$$

$$\frac{\partial^2\theta_p}{\partial\eta^2}+\frac{1-\phi}{2}g\frac{\partial\theta_p}{\partial\eta} =(1-\phi)x\left(\frac{\partial g}{\partial\eta}\frac{\partial\theta_p}{\partial x}-\frac{\partial g}{\partial x}\frac{\partial\theta_p}{\partial\eta}\right) -H\gamma x\left(\theta_f-\theta_p\right) \quad (1.13)$$

subjected to the new boundary conditions

$$f=g=0,\qquad \theta_f=\theta_p=1 \text{ on } \eta=0,$$
$$\frac{\partial f}{\partial\eta},\frac{\partial g}{\partial\eta}\to 0,\qquad \theta_f,\theta_p\to 0 \text{ as } \eta\to\infty. \quad (1.14)$$

where $f(x,\eta)$ and $g(x,\eta)$ are the similar velocities (for macrophase and microphase) and θ is the dimensionless temperature.

Here Ra represents the Rayleigh number, σ_f is an inter-phase momentum transfer parameter, β defines a modified thermal diffusivity ratio and K_r is the permeability ratio. Moreover, G_f^* and G_p^* are the inertial parameters and γ represents a modified thermal conductivity ratio. Their expressions are given by:

$$Ra=\frac{\rho g\hat{\alpha}(T_w-T_\infty)K_f L(\rho c)_f}{\phi\mu k_f},\quad \sigma_f=\frac{\zeta K_f}{\mu},$$
$$\beta=\frac{(1-\phi)k_p(\rho c)_f}{\phi\, k_f(\rho c)_p},\quad K_r=\frac{K_p}{K_f},$$
$$\theta_F=\frac{\phi\theta_f+(1-\phi)\mathcal{E}\theta_p}{\phi+(1-\phi)\mathcal{E}},$$
$$G_f^*=RaG_f\,, G_p^*=RaG_p, \gamma=\frac{\phi k_f}{(1-\phi)k_p},$$
$$H=\frac{\hat{h}}{Ra},\tau=\frac{\phi}{\phi+(1-\phi)\mathcal{E}}. \quad (1.15)$$

The solution of Eqs. (1.10) to (1.14) was obtained using an algorithm based on the routine bvp4c from Matlab combined with the discretization of the derivatives with respect to x using the first order upwind finite differences (see, [6]). The numerical experiments were performed on the computer cluster Kotys, [7]. In our simulations the following fixed values were taken into account: $\phi = \mathcal{E} = 0.4$, so that $\tau = 0.625$.

Values of the Nusselt numbers become defined as follow:

$$x^{1/2}\,Ra_x^{\,-1/2}Nu_f = -\left(\frac{\partial\theta_f}{\partial\eta}\right)_{\eta=0}, \qquad x^{1/2}Ra_x^{\,-1/2}\,Nu_p = -\left(\frac{\partial\theta_p}{\partial\eta}\right)_{\eta=0}, \tag{1.16}$$

are given in Tables 2 and 3 for the particular case when $x = 0$.

K_r	G_p^*	G_f^*	$\beta = 1$		$\beta = 10$	
			$\sigma_f = 10^{-4}$	$\sigma_f = 1$	$\sigma_f = 10^{-4}$	$\sigma_f = 1$
10^{-1}	0	0	0.3025	0.2225	0.3053	0.2325
		0.5	0.2645	0.2115	0.2710	0.2210
		1	0.2448	0.2034	0.2511	0.2125
	1	0	0.3027	0.2216	0.3094	0.2323
		0.5	0.2650	0.2109	0.2710	0.2208
		1	0.2452	0.2029	0.2511	0.2123
1	0	0	0.2768	0.2768	0.2976	0.2976
		0.5	0.2444	0.2534	0.2615	0.2706
		1	0.2279	0.2394	0.2429	0.2546
	1	0	0.2836	0.2576	0.2979	0.2927
		0.5	0.2498	0.2405	0.2617	0.2674
		1	0.2325	0.2293	0.2431	0.2522

Table 2. Values related to the dimensionless Nusselt numbers for the *f*-phase

K_r	G_p^*	G_f^*	$\beta = 1$		$\beta = 10$	
			$\sigma_f = 10^{-4}$	$\sigma_f = 1$	$\sigma_f = 10^{-4}$	$\sigma_f = 1$
10^{-1}	0	0	0.0875	0.1167	0.0290	0.0333
		0.5	0.0904	0.1158	0.0291	0.0332
		1	0.0918	0.1151	0.0292	0.0331
	1	0	0.0842	0.1093	0.0287	0.0332
		0.5	0.0862	0.1086	0.0290	0.0331
		1	0.0875	0.1081	0.0291	0.0329
1	0	0	0.3559	0.3559	0.1291	0.1291
		0.5	0.3615	0.3426	0.1303	0.1275
		1	0.3644	0.3349	0.1309	0.1266
	1	0	0.2698	0.2888	0.1266	0.1275
		0.5	0.2738	0.2834	0.1276	0.1262
		1	0.2759	0.2800	0.1282	0.1254

Table 3. Values related to the dimensionless Nusselt numbers for the *p*-phase

For the case $x \neq 0$, the variation of the fluid flow and heat transfer characteristics is shown in Figs. 2 to 5 for $\sigma_f = 10^{-4}$, $\beta = 2.8279$, $K_r = 0.1$ and $\tau = 0.625$.

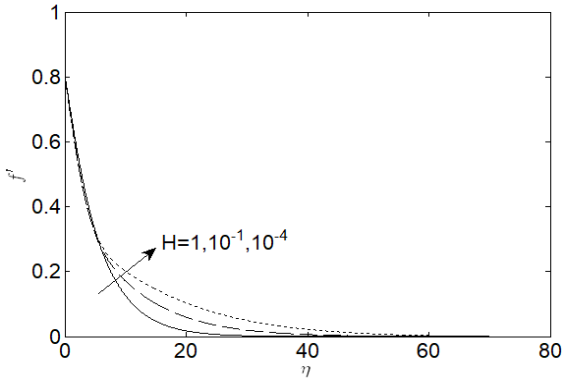

Fig. 2. Variation of $f'(\eta)$ with H for $G_f^* = 0.3$, $G_p^* = 0.2$, $x = 0.25$ and $\gamma = 0.4013$.

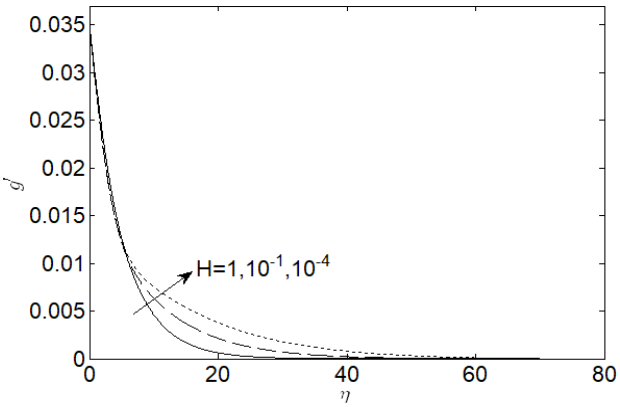

Fig. 3. Variation of $g'(\eta)$ with H for $G_f^* = 0.3$, $G_p^* = 0.2$, $x = 0.25$ and $\gamma = 0.4013$.

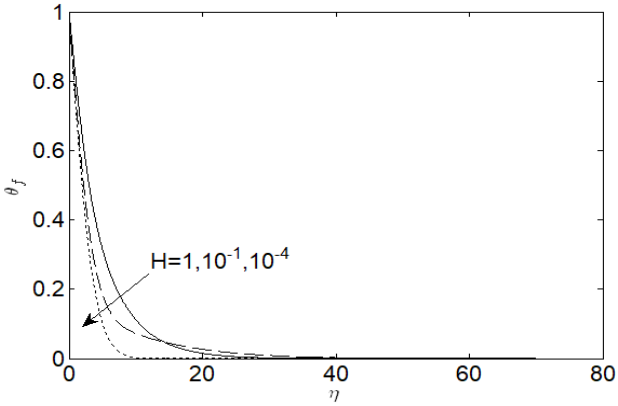

Fig. 4. Variation of $\theta_f(\eta)$ with H for $G_f^* = 0.3$, $G_p^* = 0.2$, $x = 0.25$ and $\gamma = 0.4013$.

The H parameter variation produces changes in the velocity and temperature profiles Decreasing the parameter generates an increase in the thickness of the dynamic boundary layers (in macro and micro phases) and thermal boundary layer in the

microphase. In macrophase the decrease of the modified inter-phase heat transfer parameter causes a dramatic decrease of the boundary layer and the heat transfer between the phases becomes negligible.

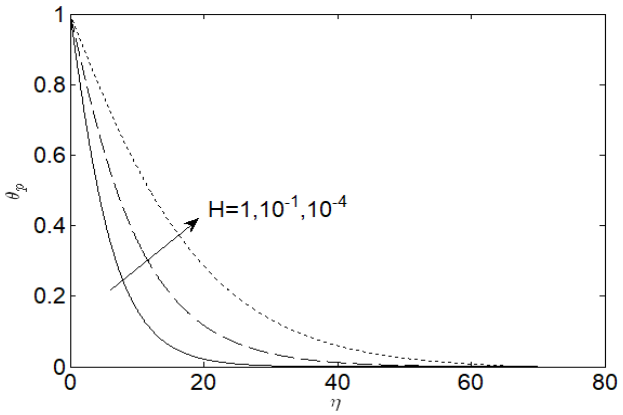

Fig.5. Variation of $\theta_f(\eta)$ (left) and $\theta_p(\eta)$ (right) with H for $G_f^* = 0.3$, $G_p^* = 0.2$, $x = 0.25$ and $\gamma = 0.4013$

2.1 Natural convection from a vertical plate embedded

Consider the natural convection flow and heat transfer inside a square cavity of width L which is filled with a BDPM porous medium taking into account the Brinkman terms (as shown in Fig. 6). It is assumed that the temperature of the right wall of the cavity is T_h and the temperature of the left wall is T_c.

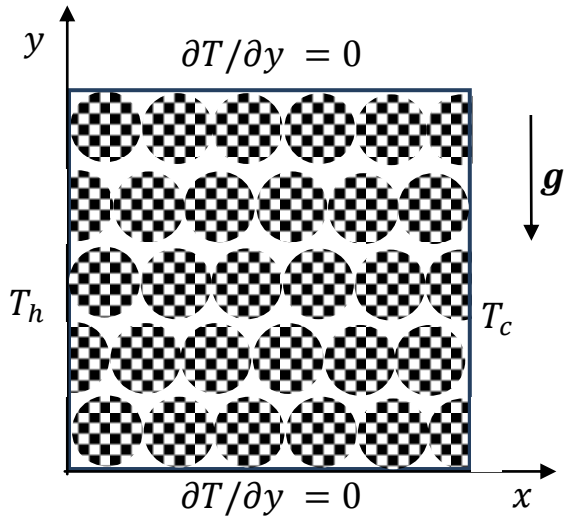

Fig. 6. Geometry of the cavity

It is worth mentioning that the similar problem for a Darcy bidisperse porous medium was solved by Revnic et al., [8]. The non-dimensional equations using the stream function – vorticity formulation are given by:

$$(1+\sigma_f)\Omega_f - \beta\sigma_f\Omega_p - Da\,\Delta\Omega_f = Ra\left(\hat{0}\frac{\partial\theta_f}{\partial X} + (1-\tau)\frac{\partial\theta_p}{\partial X}\right) \quad (1.17)$$

$$-\sigma_f\Omega_f + \beta\left(\frac{1}{K_r}+\sigma_f\right)\Omega_p - Da\,\Delta\Omega_p = Ra\,(\,\tau\frac{\partial\theta_f}{\partial X} + (1-\tau)\frac{\partial\theta_p}{\partial X}) \quad (1.18)$$

$$\Delta\theta_f = \phi\left(\frac{\partial\psi_f}{\partial Y}\frac{\partial\theta_f}{\partial X} - \frac{\partial\psi_f}{\partial X}\frac{\partial\theta_f}{\partial Y}\right) + H(\theta_f - \theta_p) \quad (1.19)$$

$$\Delta\theta_p = (1-\phi)\left(\frac{\partial\psi_p}{\partial Y}\frac{\partial\theta_p}{\partial X} - \frac{\partial\psi_p}{\partial X}\frac{\partial\theta_p}{\partial Y}\right) + H\,\gamma(\theta_p - \theta_f) \quad (1.20)$$

$$\Delta\,\psi_f = -\,\Omega_f \quad (1.21)$$

$$\Delta\,\psi_p = -\,\Omega_p \quad (1.22)$$

along with the boundary conditions

$$\psi_f = \psi_p = 0,\ \theta_f = \theta_p = \frac{1}{2} \text{ at } X = 0 \quad (1.23)$$

$$\psi_f = \psi_p = 0,\ \theta_f = \theta_p = -\frac{1}{2} \text{ at } X = 1 \quad (1.24)$$

$$\psi_f = \psi_p = 0,\quad \frac{\partial\theta_f}{\partial Y} = \frac{\partial\theta_p}{\partial Y} = 0 \text{ at Y} = 0 \text{ and } Y = 1 \quad (1.25)$$

Here Ω, ψ and θ are the dimensionless vorticity, stream function and temperature, while , $Da = \frac{\tilde{\mu}\ K_f}{\mu\ L^2}$ is the Darcy number. The physical quantities of interest are the local Nusselt numbers given by

$$Nu_f = -\left(\frac{\partial\theta_f}{\partial X}\right)_{X=0},\quad Nu_p = -\left(\frac{\partial\theta_p}{\partial X}\right)_{X=0} \quad (1.26)$$

Equations (1.17) to (1.25) were solved numerically using a finite difference discretization along with a Gauss–Seidel iteration technique. The used error was 10^{-9}. A grid dependency test was perform, and finally a 101x101 was chosen. For the case of the monodispersed porous medium the numerical results were compared with results from the open literature, [8], the agreement being very good.

Streamlines and isotherms were obtained for different values of the governing parameters. However, because we considered the Brinkman

terms in the momentum equations we focused on the effect of the Darcy number on the flow and heat transfer characteristics. In the simulation the following values for the governing parameters were considered: *Ra=1000*, $\gamma = 1$ and $H = 0.05$. The variation of the streamlines and isotherms with *Da* is depicted in Figs 7 and 10. One can notice that an increase in *Da* leads to a slight modification in macrophase streamlines, the effect being more present in microphase. A modification of the isotherm modification is also visible in macrophase, while in microphase the effect is insignificant.

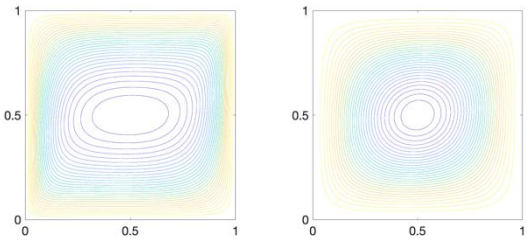

Fig. 7. Macrophase streamlines for *Da=0.001*(left) and *Da=0.1* (right)

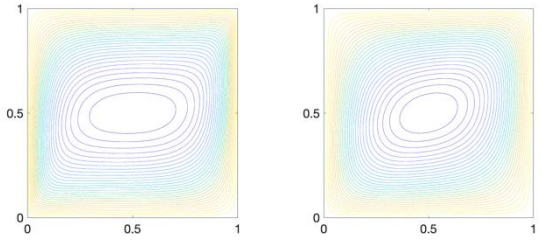

Fig. 8. Microphase streamlines for *Da=0.001*(left) and *Da=0.1* (right)

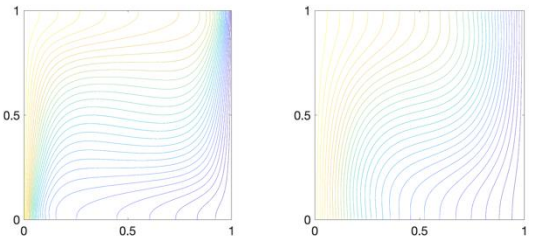

Fig. 9. Macrophase isotherms for *Da=0.001*(left) and *Da=0.1* (right)

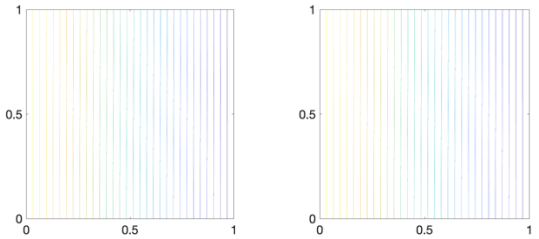

Fig. 10. Microphase isotherms for *Da=0.001*(left) and *Da=0.1* (right)

Acknowledgements

The authors would like to acknowledge the financial support received from the grant PN-III-P4-ID-PCE-2016-0036, UEFISCDI of Romanian Ministry of Sciences.

References:

[1] Nield, D.A., Bejan, A., *Convection in Porous Media* (5th ed). Springer, New York, 2017.

[2] Straughan, B., *Convection with Local Thermal Non-Equilibrium and Microfluidic Effects*, Springer, Heidelberg, 2015.

[3] Szczygieł, J., Enhancement of reforming efficiency by optimising the porous structure of reforming catalyst: Theoretical considerations, *Fuel*, Vol. 85, 2006, pp. 1579–1590.

[4] Lin, F.-C., Liu, B.-H., Juan C.-C., Chen, Y.-M., Effect of pore size distribution in bidisperse wick on heat transfer in a loop heat pipe, *Heat Mass* Transfer, Vol. 47, 2011, pp. 933–940.

[5] Shi J.Q., Durucan S., Gas storage and flow in coalbed reservoirs: Implementation of a bidisperse pore model for gas diffusion in a coal matrix, *SPE Reservoir Evaluation & Engineering*, Vol.8, 2005, pp. 169-175.

[6] Patrulescu,, F.O., Grosan, T., Pop, I. Natural convection from a vertical plate embedded in a non-Darcy bidisperse porous medium, *Journal of Heat Transfer*, (in press), 2019, DOI: 10.1115/1.4045067

[7] Bufnea, D., Niculescu, V., Silaghi, Gh., Sterca, A., Babeş-Bolyai university's high performance computing center, *Studia Universitatis Babes-Bolyai Informatica*, Vol. 61, 2016, pp. 54 – 69.

[8] Revnic C., Grosan, T., Pop, I., Ingham, D.B., Free convection in a square cavity filled with a bidisperse porous medium, *International Journal of Thermal Science.*, Vol. 48, 2009, pp. 1876-1883.